Ultrathin carbon nanotube with single, double and triple bonds
Supplemental material

E. Menéndez-Proupin,[1] Ana L. Montero-Alejo,[2] and J. M. García de la Vega[1]

[1]*Departamento de Química Física Aplicada, Facultad de Ciencias, Universidad Autónoma de Madrid, 28049 Madrid, Spain*

[2]*Laboratorio de Química Computacional y Teórica, Facultad de Química, Universidad de la Habana, 10400 Havana, Cuba*

Abstract

This document contain details of the computational methods, as well as additional data of the electronic structure and optical properties. It also contains the patterns of the infrared and Raman active phonons, and a description of the structure considered as a double carbon chain.

I. COMPUTATIONAL DETAILS

Density functional theory (DFT) calculations have been performed using a plane-wave pseudopotential scheme as implemented in QUANTUM ESPRESSO[1]. The exchange and correlation parts of the electronic energy were calculated in the generalized gradient approximation (GGA) with the functional of Perdew, Burke and Ernzerhof (PBE)[2]. The effects of the core electrons and nuclei are included using the Rabe-Rappe-Kaxiras-Joannopoulos[3] type ultrasoft pseudopotential `C.pbe-rrkjus.UPF` included in the QUANTUM ESPRESSO distribution. Kinetic energy cutoffs of 30 and 320 Ry have been used for the expansion of the wavefunctions and the charge density, respectively. The one-dimensional Brillouin zone was sampled using a shifted uniform grids of 14 k-points. In order to avoid convergence problems in some 'metallic' configurations, the method of cold smearing[4] with a broadening parameter of 0.01 Ry was used. In a recent work[5] on CNT's we have probed that the selected cutoffs, k-point grid, and smearing scheme, allow to obtain energies, forces, and stresses converged within 0.01 eV/atom, 0.05 eV/angstrom and 0.5 kbar, respectively. The supercell enclosing the CNT has a fixed transversal size of 18 Å, and variable size along the CNT axis that is 11.15 Å for the converged CNT10R structure. For density of states (DOS) calculations, a Gaussian smearing of 0.02 eV and a $\Gamma-$centered grid of 60 k-points have been used. The IR and Raman spectra have been calculated using density functional perturbation theory[6] as implemented in the PHonon code of QUANTUM ESPRESSO. This framework provides accurate phonon frequencies that in the worst cases differ in 50 cm^{-1} from the experiments. Nonetheless, the average accuracy is far better[6]. The local density approximation was used, with the norm conserving pseudopotential `C.pz-vbc.UPF` and a plane wave cutoff of 60 and 240 Ry for the wavefunctions and density, respectively. For testing purposes we have computed the IR spectrum for a zigzag CNT (8,0) and we have obtained an IR spectrum consistent with the results of Ref. 7. The frequencies of the IR active modes coincide within 1 % and the relative intensities follow the same pattern, the A_{2u} intensity being 121 and 1.4×10^4 times stronger than the LF-E_{1u} and HF-E_{1u} ones, respectively.

The optical absorption spectrum has been calculated with the linear response time-dependent DFT (TDDFT) as implemented in the `turboTDDFT` code[8]. 4000 Lanczos iterations were computed for each spectra, and 6000 additional coefficients are obtained by

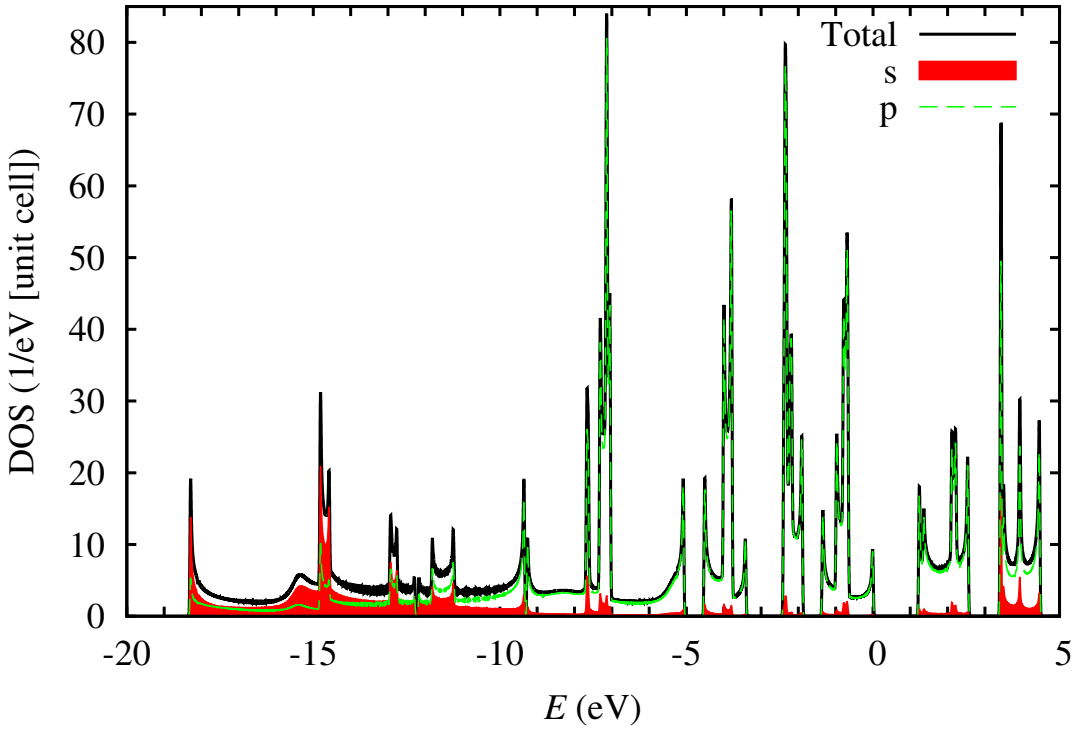

FIG. 1: (Color online) Density of states of CNT10R structure in extended range. Zero energy is the Fermi level.

extrapolation. A half width at half maximum parameter of 0.1 eV was used to broaden the spectra. As the `turboTDDFT` code only allows to compute gamma point wavefunctions, used a seven-units supercell, equivalent to a $1 \times \times 7$ k-points mesh. This sampling is not enough to obtain a fully converged spectrum, but it produces converged positions and intensities of the main peaks. We have proved that this is the case by performing control simulations with five-units and eight-units supercells. Results show that some shoulders of the main peaks change between the 7-units and 8-units supercell. We have also made tests of convergence using the spectra calculated in the single-particle approximation, that can be done with any sampling of the Brillouin zone.

The molecular dynamics simulations were carried out using the General Utility Lattice Package (GULP) [9]. The simulations have been in the NVT ensemble with of Nose-Hoover thermostat parameter of 0.005. The equation of motion was integrated with the leapfrog algorithm and a time step of 1 fs.

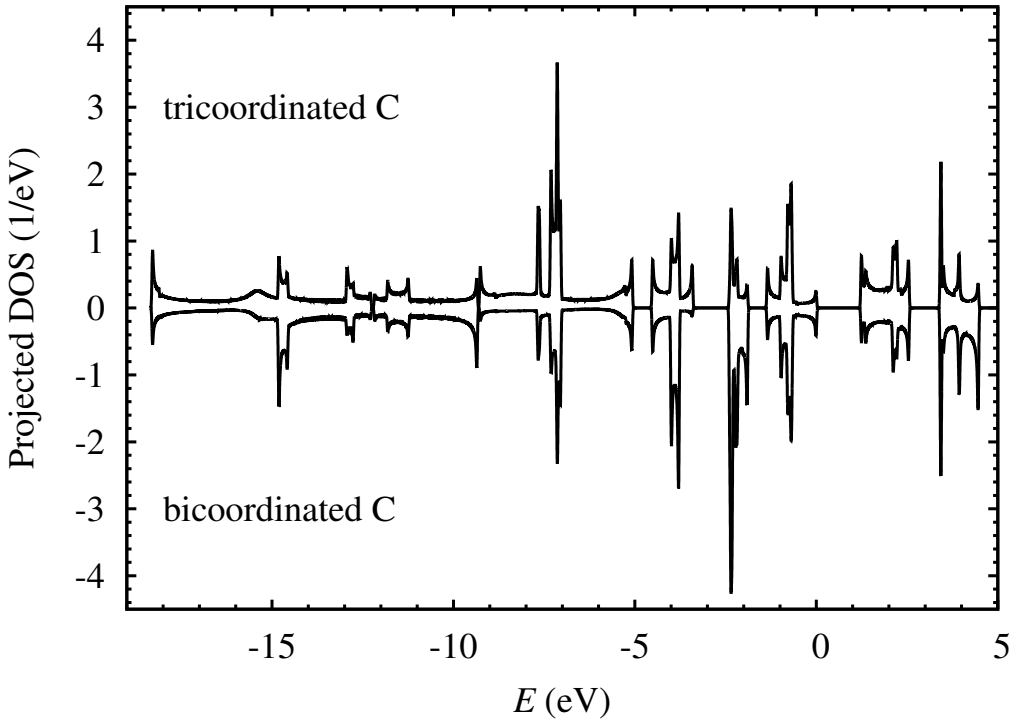

FIG. 2: Density of states of CNT10R structure projected on tri-coordinated and bi-coordinated carbons. Zero energy is the Fermi level.

II. ELECTRONIC STRUCTURE

Figure 1 shows the projected density of states (DOS) over $2s$ and $2p$ atomic orbitals. It shows that between -11 eV and 3 eV DOS is dominated by $2p$ states. Out of this range, $2s$ states contribute significantly and dominate DOS peaks at -18.3,-14.8, and -14.6 eV.

Fig. 2 shows the atom-projected DOS on tri- and bi-coordinated carbons. The largest imbalance is in favor of bi-coordinated carbons at -2.35 eV, and in favor of tri-coordinated carbons at -7.13 eV. This imbalance might help to differentiate both types of carbons by scanning tunneling microscopy.

A. Charge density and electron localization function

The valence charge density isosurfaces are shown in Fig. 3. The high density isosurfaces locate around the bonding lines, taking the highest values around the bonds between bicoordinated carbons. This is an indication of a multiple bond, although it may also be

a consequence of the proximity of both atoms. One obvious question is the satisfaction of the valence rules. The calculation of the spin density shows negligible values (absolute integrated values of 0.01 Bohr magneton) that can be attributed to controlled numerical error. This means that there is no unpaired electron state.

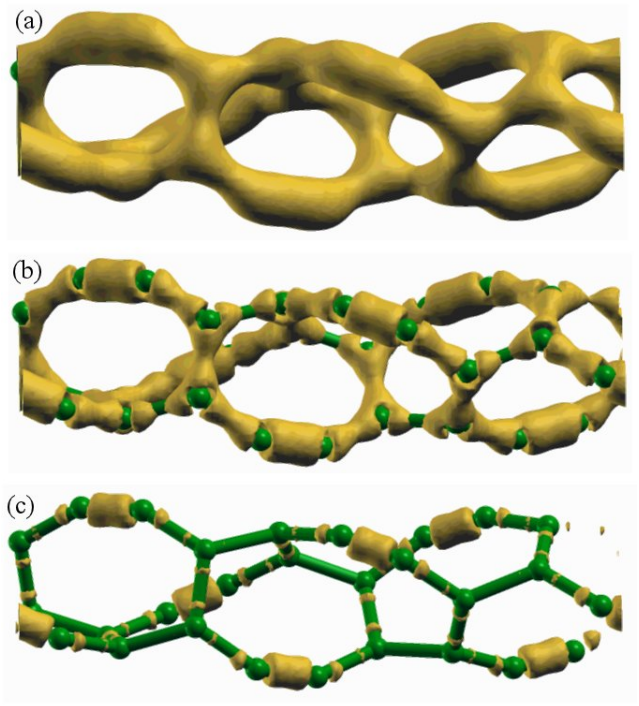

FIG. 3: Charge density isosurfaces. Density values: (a) 0.2 au, (b) 0.25 au, (c) 0.3 au.

The isosurfaces of the electron localization function (ELF)[10, 11] isosurfaces are shown in Fig. 4. Spatial regions with high values of the ELF indicate paired electrons, such as covalent bonds and lone pairs. In Fig. 4 the clouds of the ELF are located around the bonding lines, indicating covalent bonds and no lone pair. The symmetry and sizes of the isosurfaces indicate qualitatively the bonding characters. One can see that the isosurfaces around the bonds ^{2}C-C^{2} and ^{2}C-C^{3} have approximately cylindrical symmetry for ELF=0.8, and that the former isosurface is much larger than the second one. This suggests a triple and a single bond at ^{2}C-C^{2} and ^{2}C-C^{3}. On the other hand, the isosurfaces around the middle of short ^{3}C-C^{3} bonds are elongated perpendicularly to the bond, indicating a π-type bond. Naturally, as the geometry deviates from the ideal hybridization geometries, the symmetry of the ELF cannot be perfect, as is shown for ELF=0.75 and 0.85. A bond order analysis in the next section provides mathematical support to this discussion.

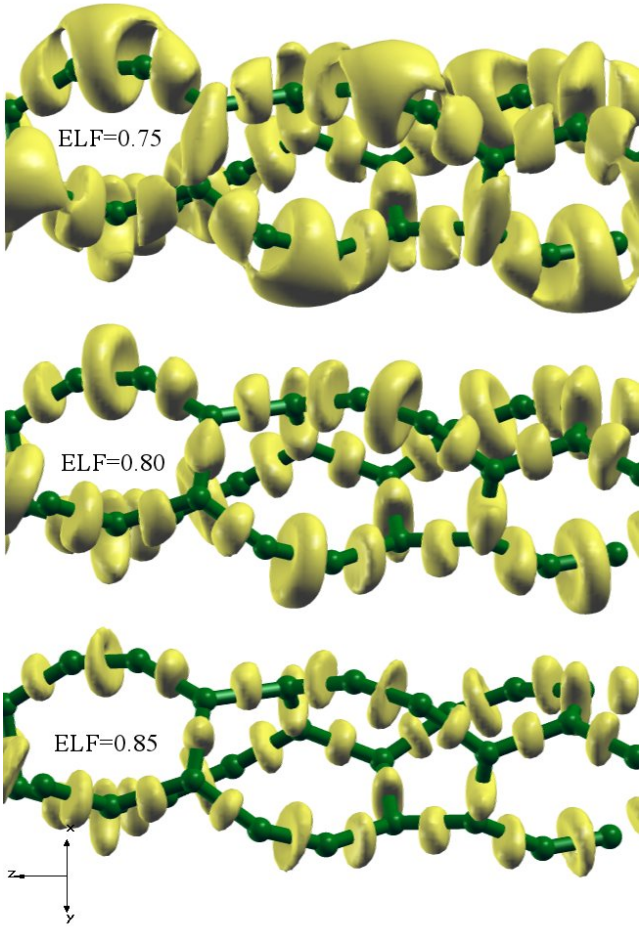

FIG. 4: Electron localization function.

B. Bond orders and charge deformations

Non-periodic hydrogen-terminated models of CNT10R and graphene were obtained by replicating the corresponding relaxed unit cells. Lengths of the CNT10R and graphene models are 4.32 and 1.97 nm, respectively. Relaxed functions of these models were obtained at PBE-PBE/6-31G level of theory. Calculations were performed with Gaussian 09 program package.[12] A bond order (BO) analysis was performed by means of the Wiberg bond index (WBI) under the natural bond orbital (NBO) description. The WBI indexes provided a numerical picture about the bond types and are used to trace the electronic conjugation in the system. The BO's show that triple, double and even single bonds coexist in the CNT10R rings. Consequently, the π electron density of this kind of CNT cannot be delocalized through the whole system as is common in graphene and other CNTs. This is also expressed

TABLE I: Carbon-carbon bond orders (BO) in CNT10R. The notation ^{n}C indicates an n-coordinated carbon. There are two cases of ^{3}C−^{3}C bonds

	^{2}C−^{2}C	^{2}C−^{3}C	^{3}C−^{3}C (short)	^{3}C−^{3}C (long)	Graphene
BL (Å)	1.23	1.41	1.43	1.49	1.42
BO	2.46	1.21	1.45	1.00	1.24

in the asymmetry in the bond length (BL). The difference in BO between long and short ^{3}C−^{3}C bonds also suggests a differentiation in single and double bonds. The fact that the ^{2}C−^{3}C BO is larger than one (in contrast with the long ^{3}C−^{3}C bond), together with the similarity in BL and BO with the case of graphene, suggests that ^{2}C−^{3}C bonds share some π delocalization with neighbor bonds.

III. POLARIZABILITY

The polarizability tensor is given by `turbo-TDDFT` in units of $e^2a_0^2/\text{eV} = 4.032306$ Å^3, where a_0 is the Bohr radius. For reference it is shown in Fig. 5. The absorption spectrum is proportional to the cross section

$$\sigma(\omega) = \frac{4\pi\omega}{c}\text{Im}\alpha_{nn}(\omega), \tag{1}$$

where $n = x, y, z$ is the direction of light polarization vector. The polarizability tensor is diagonal.

As the calculation has been performed with periodic boundary conditions, the polarizability given by `turbo-TDDFT` is in fact

$$4\pi n\alpha = \epsilon - 1, \tag{2}$$

where n is the particle density, i.e., the inverse of the supercell volume, and ϵ is the effective dielectric function of periodic array of nanotubes. Both α and ϵ are frequency-dependent complex functions.

The dielectric function relates with the polarizability of individual molecules α_1 by the Clausius-Mossotti, that can be cast as

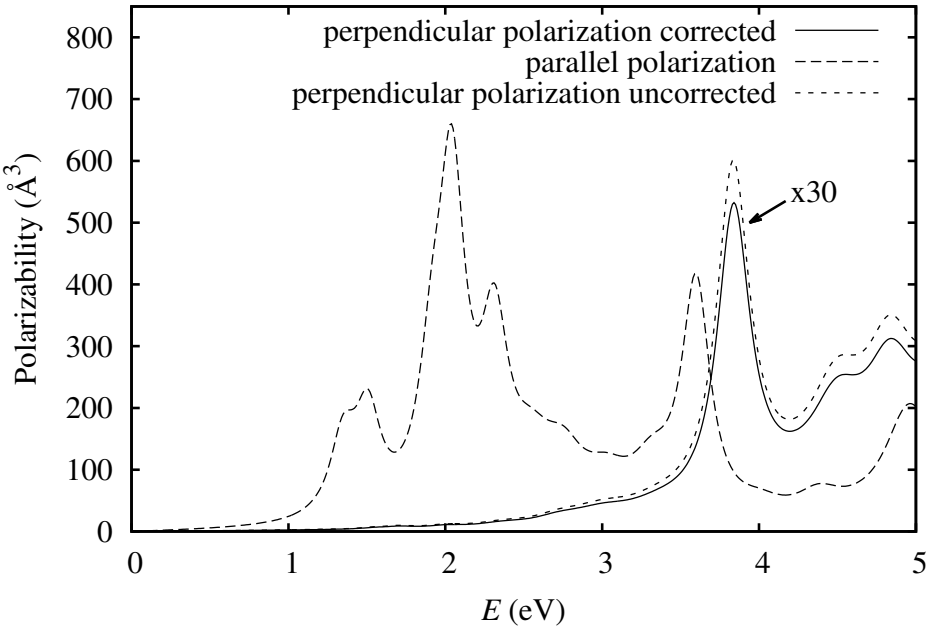

FIG. 5: Polarizability per unit cell of CNT10R.

$$4\pi n\alpha_1 = \frac{\epsilon - 1}{1 + N_p(\epsilon - 1)}, \tag{3}$$

where N_p is the depolarization factor. For cylindrical geometry and parallel polarization $N_p = 0$ and no correction is needed.

$$\alpha_{1,\parallel} = \alpha_{\parallel}. \tag{4}$$

For perpendicular polarization $N_p = 1/2$. Hence

$$\alpha_{1,\perp} = \frac{\alpha_{\perp}}{1 + 4\pi N_p \alpha_{\perp}}. \tag{5}$$

The corrected and uncorrected polarizability are shown in Fig. 5.

IV. VIBRATIONAL MODES

Tables II and III display the amplitudes of vibration of the IR and Raman active vibrational modes.

TABLE II: IR active modes.

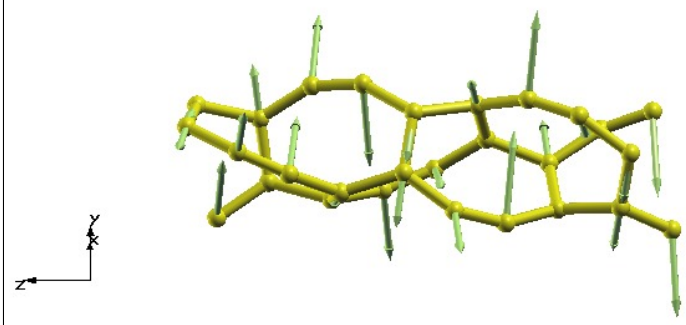
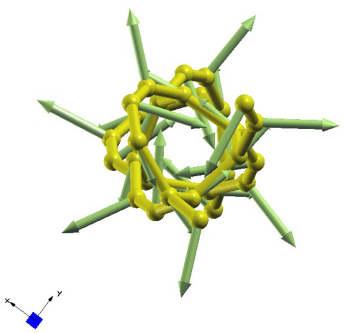

Mode 11, 279 cm^{-1}

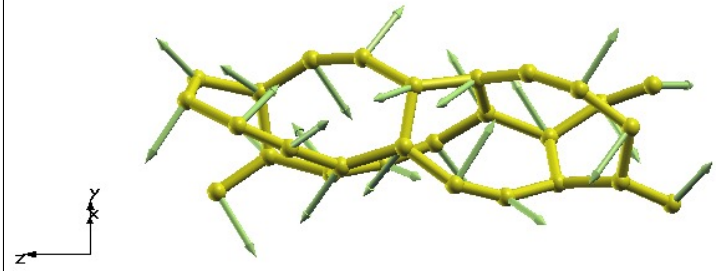
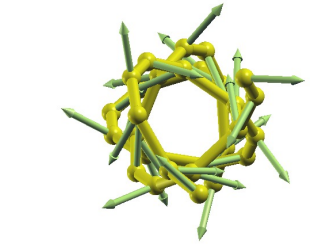

Mode 29, 488 cm^{-1}

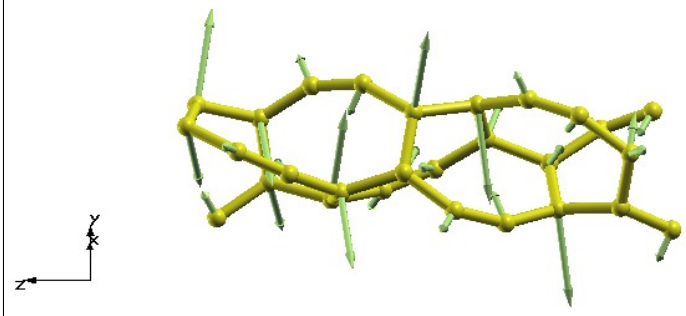
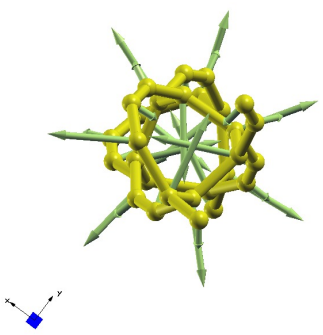

Mode 50, 711 cm^{-1}

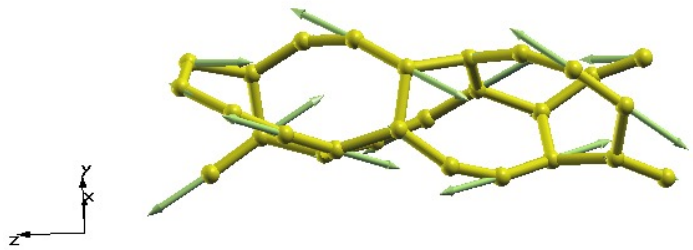 Mode 70, 1293 cm^{-1}	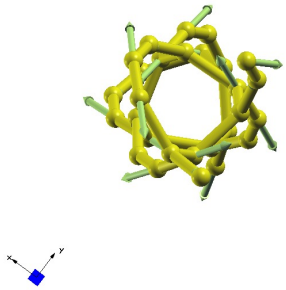

TABLE III: Raman active modes.

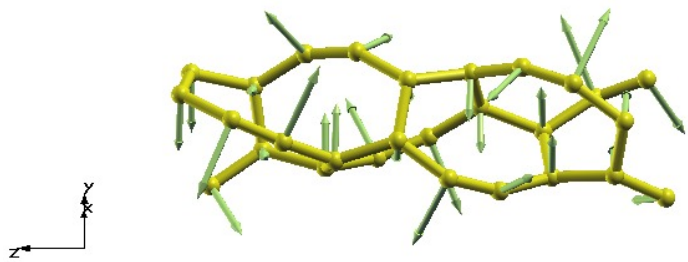 Mode 22, 411 cm^{-1}	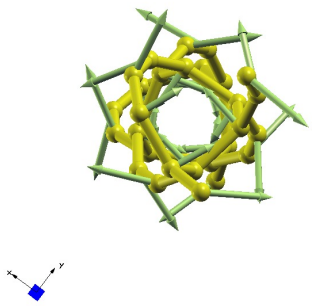
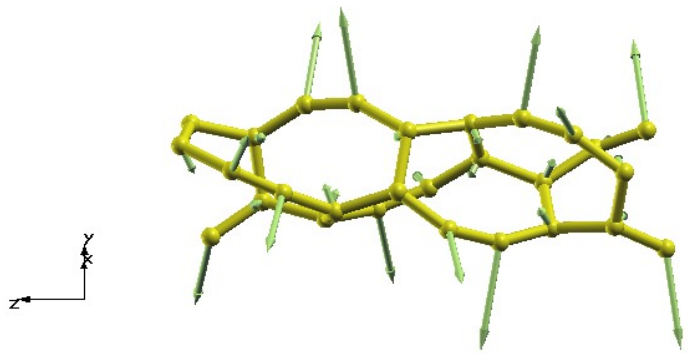 Mode 32, 537 cm^{-1}	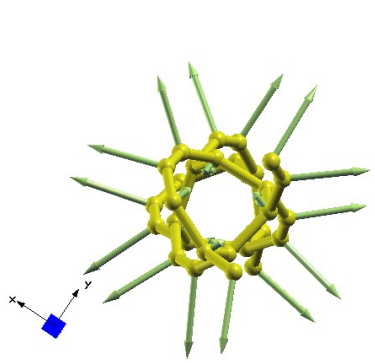

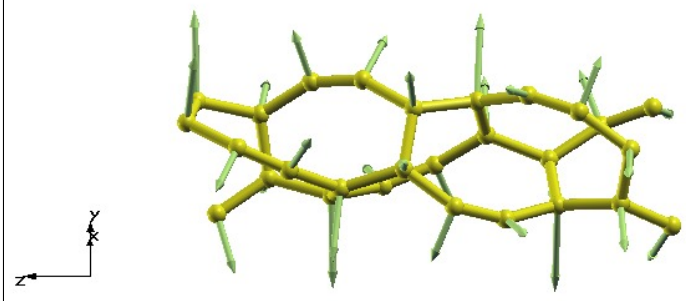
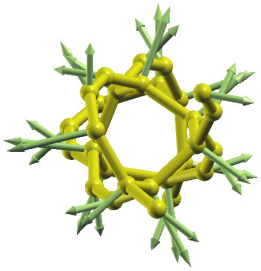

Mode 47, 690 cm^{-1}

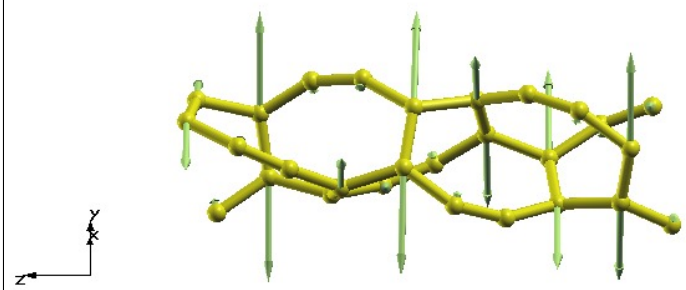
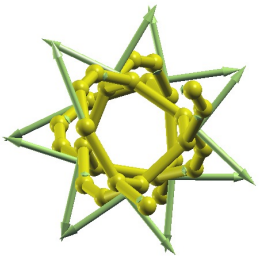

Mode 63, 1201 cm^{-1}

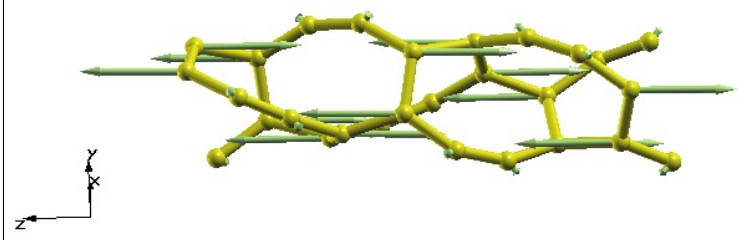
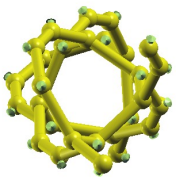

Mode 71, 1297 cm^{-1}

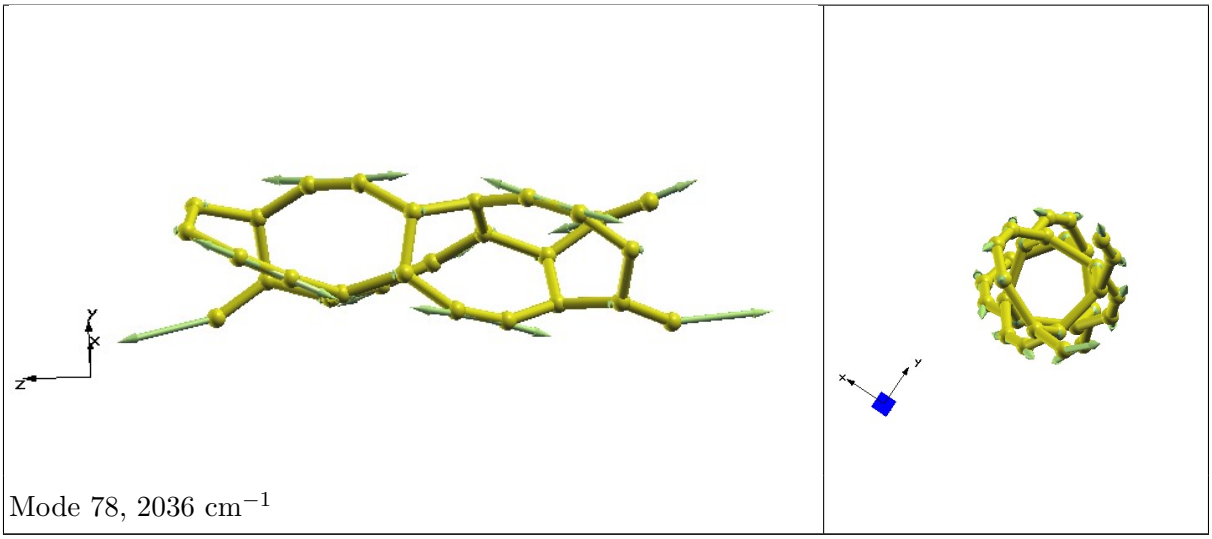

The Raman mode at 2036 cm^{-1} deserves a special attention. This frequency is typical of triple bond stretching, in agreement with the above mentioned descriptors of the electronic structure.

V. DOUBLE CHAIN MODEL

The CNT10R structure can be understood as a pair of intertwined chains of carbons with alternating single (S), double (D) and triple (T) bonds. Each chain is represented in Fig. 6 with a different color. The bond multiplicity sequence is (STS)D(STS)D.... Denoting the carbons by their coordination, the full sequence is specified as (3S2T2S3)D(3S2T2S3)D..., and can be regarded a hybrid polyyne-cumulene chain.[13, 14] The chains are stabilized by bridging single bonds, indicated in Fig. 6 by two-color sticks. The individual chains has a period of a double unit cell, i.e., 22.308 Å. Each period contains seven units (3S2T2S3)D of each chain. The D bonds make a turn of 180° in the chain period, averaging to 25.7° between consecutive positions. Of this amount, 6.0° in average correspond to dihedral angles of the (3S2T2S3) subunits. The bond multiplicities are idealized in this picture, the bond angles along the chains are not 180° and 120° and some amount of bond order is transferred from the T to the adjacent S bonds.

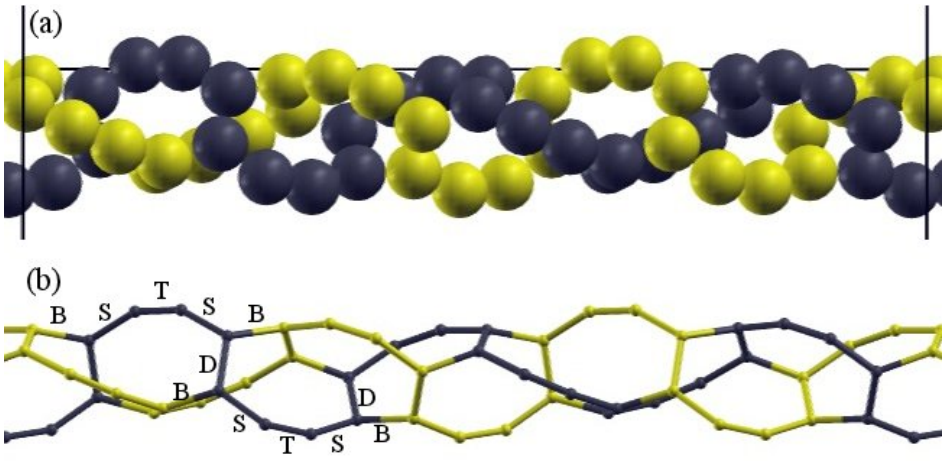

FIG. 6: Double chain model of CNT10R.(a) Ball view. (b) Ball and sticks view with indication of single (S), double (D), triple (T) and bridging (B) bonds.

---

[1] P. Giannozzi, S. Baroni, N. Bonini, M. Calandra, R. Car, C. Cavazzoni, D. Ceresoli, G. L. Chiarotti, M. Cococcioni, I. Dabo, et al., J. Phys.: Condens. Matter **21**, 395502 (2009).

[2] J. P. Perdew, K. Burke, and M. Ernzerhof, Phys. Rev. Lett. **77**, 3865 (1996).

[3] A. M. Rappe, K. M. Rabe, E. Kaxiras, and J. D. Joannopoulos, Phys. Rev. B **41**, 1227 (1990).

[4] N. Marzari, D. Vanderbilt, A. D. Vita, and M. C. Payne, Phys. Rev. Lett. **82**, 3296 (1999).

[5] A. L. Montero-Alejo, M. E. Fuentes, E. Menéndez-Proupin, W. Orellana, C. F. Bunge, L. A. Montero, and J. M. G. de la Vega, Phys. Rev. B **81**, 235409 (2010).

[6] S. Baroni, S. de Gironcoli, A. Dal Corso, and P. Giannozzi, Rev. Mod. Phys. **73**, 515 (2001).

[7] J. Zhou and J. Dong, J. Appl. Phys. **107**, 024306 (2010).

[8] O. B. Malcıoğlu, R. Gebauer, D. Rocca, and S. Baroni, Comput. Phys. Commun. **182**, 1744 (2011).

[9] J. Gale and A. Rohl, Mol. Simul. **29**, 291 (2003).

[10] A. D. Becke and K. E. Edgecombe, J. Chem. Phys. **92**, 5397 (1990).

[11] A. Savin, O. Jepsen, J. Flad, O. Andersen, H. Preuss, and H. G. von Schnering, Angew. Chem. Int. Ed. Engl. **31**, 187 (1992).

[12] M. J. Frisch et al, Gaussian 09, Revision A.1, Gaussian, Inc.: Wallingford CT, 2009.

[13] L. Ravagnan, N. Manini, E. Cinquanta, G. Onida, D. Sangalli, C. Motta, M. Devetta, A. Bor-

doni, P. Piseri, and P. Milani, Phys. Rev. Lett. **102**, 245502 (2009).

[14] G. Moras, L. Pastewka, M. Walter, J. Schnagl, P. Gumbsch, and M. Moseler, J. Phys. Chem. C **115**, 24653 (2011).